Baseband Model for Symmetric PWM Modulator: Frequency Analysis and THD

Fernando Chierchie†1 and Eduardo E. Paolini†2

† *"Instituto de Investigaciones en Ing. Eléctrica (IIIE) Alfredo Desages" (UNS-CONICET), Depto. de Ing. Eléctrica y de Computadoras. Universidad Nacional del Sur Av. Alem 1253, 8000 Bahía Blanca, Argentina*

1 fernando.chierchie@uns.edu.ar   2 epaolini@uns.edu.ar

***Abstract*—Accurate models for PWM modulators composed by the parallel connection of p-th order powers followed by a linear filter have been recently presented in the literature. In this paper we derive closed-form expressions for the impulse responses and frequency responses of those filters. This allows to predict the amplitudes and frequencies of the spurious components appearing in the baseband when using sinusoidal inputs and also to obtain a closed-form expression for the THD.**

***Resumen*— Recientemente se han presentado en la literatura modelos precisos para moduladores PWM compuestos por la conexión en paralelo de potencias de orden p seguido de un filtro lineal. En este trabajo se derivan expresiones cerradas para las respuestas impulsivas y respuestas en frecuencia de los filtros. Esto permite predecir las amplitudes y frecuencias de las componentes espurias que aparecen en la banda base cuando se utilizan entradas sinusoidales y también obtener una expresión cerrada para la distorsión armónica total.**

I. Introduction

Pulse width modulation (PWM) has a wide range of applications, from power electronics in energy conversion [1], to audio switching amplifiers [2] and RF power amplifiers [3] among others.

Discrete-time nonlinear models that capture the behavior of digital pulse width modulation in the frequency range between DC and half the PWM frequency (baseband) have been recently presented [4]–[7]. These models are developed from a time-domain perspective and accurately expos the relation between the duty cycles and the samples of the bandlimited PWM signal. The model is composed of the parallel connection of an static nonlinearity (power of the input) and a linear filter conforming an structure known as parallel Hammerstein.

Frequency analysis to obtain the spectra of PWM signals have also been presented, for sinusoidal modulating signals [1] and also for arbitrary, bounded, bandlimited modulating signals [8]. In this paper, we derive closed-form formulas for the impulse and frequency responses of the linear filters of the PWM model. For sinusoidal inputs this model allows to individualize the frequency and the amplitudes of the spurious distortion components that appear in baseband due to the PWM modulation. The mechanism by which the "aliasing distortion" [3], [9]–[11] of the PWM modulator is generated is also revealed.

An analytic expression for the total harmonic distortion (THD) as a function of input amplitude (modulation index) and input frequency is presented. Under typical operating conditions we show that distortion is directly proportional to the modulation index and to the square of the input frequency. These results are compared with a numerical simulations of the PWM modulator.

The paper is organized as follows: in Section II the model for the PWM signal is reviewed and formulas for the impulse responses and their frequency response are given. The analysis in the frequency domain is presented in Section III and the simulations in Section IV.

II. Discrete-time nonlinear model for the digital PWM modulator

Models for different types of digital PWM have been recently presented in the literature [5], [7]. In this section we briefly summarize one of those models and introduce explicit expressions for the impulse responses of the digital filters.

We assume that a discrete-time input signal $-1 \leq x_n \leq 1$ is mapped into the duty-cycles w_n as

$$w_n = \frac{(1 + x_n)}{2} \tag{1}$$

which gives 0% duty-cycle for $x_n = -1$ and 100% for $x_n = 1$. This affine relation between the samples of the input signal and the duty cycles is typical of uniform PWM (UPWM). In practical applications UPWM is performed comparing a digital value of w_n with an ascending/descending digital counter.

The PWM signal $q(t)$ is a two level signal taking values 0 and 1 composed of symmetric pulses centered at $T = 1/f_s$ with width $w_n T$. We assume, without loss of generality that $T = 1/f_s = 1$.

To derive the model the signal $q(t)$ is filtered with an ideal low pass-filter with cut-off frequency $f_s/2 = 0.5$ and impulse response

$$r(t) = \operatorname{sinc}(t) = \frac{\sin(\pi t)}{\pi t}, \tag{2}$$

giving as result the bandlimited signal $y(t)$. The discrete-time signal y_n results from sampling $y(t)$ at f_s [7]

$$y_n = \sum_{u=1}^{\infty} h_{2u-1,n} * (w_n)^{2u-1} \tag{3}$$

where $*$ indicates the discrete-time convolution and $h_{p,n}$ are the impulse responses of discrete-time filters. Due to the symmetry of the pulses of the PWM signal only odd powers of the duty cycles appear in (3). The discrete-time

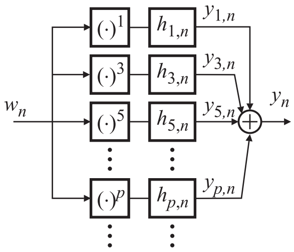

Fig. 1. Discrete baseband model of the PWM modulator.

signal y_n computed with (3) represents exactly the baseband content of the PWM signal $q(t)$. A block diagram for the computation of y_n is shown in Fig 1. This structure is known as general o parallel Hammerstein model, where each branch is composed of an static nonlinearity (power) followed by a linear filter.

The impulse responses $h_{p,n}$ can be computed as

$$h_{p,n} = \frac{1}{p!2^{p-1}} r^{(p-1)}(nT) \tag{4}$$

where $r^{(p)}(\cdot)$ is the p-times derivative of $r(t)$. Explicit expressions for $h_{p,n}$ as a function of n and for different values of p can be calculated by computing the $p-1$ derivative of $r(t)$ and by evaluating equation (4). This expressions were tabulated for some values of p in [5], [7]. For example for $p = 3, 5$, and 7 they are given by

$$\begin{aligned} h_{3,n} &= \begin{cases} -\frac{(-1)^n}{12n^2}, & \text{if } n \neq 0, \\ -\pi^2/72, & \text{if } n = 0, \end{cases} \\ h_{5,n} &= \begin{cases} \frac{(-1)^n(-6+n^2\pi^2)}{480n^4}, & \text{if } n \neq 0, \\ \pi^4/9600, & \text{if } n = 0, \end{cases} \\ h_{7,n} &= \begin{cases} -\frac{(-1)^n(120-20n^2\pi^2+n^4\pi^4)}{53760n^6}, & \text{if } n \neq 0, \\ -\pi^6/2257920, & \text{if } n = 0. \end{cases} \end{aligned} \tag{5}$$

In the Appendix it is shown that a closed-form equation for $h_{p,n}$ is given by

$$h_{p,n} = \begin{cases} \frac{j(-1)^{n+p}}{p\pi 2^p n^p} \sum_{u=0}^{p-1} \frac{(j\pi n)^u}{u!} \left((-1)^u - 1\right), & \text{if } n \neq 0, \\ \frac{1}{pp!} \left(\frac{\pi}{2}\right)^{p-1} \sin\left(\frac{p\pi}{2}\right), & \text{if } n = 0. \end{cases} \tag{6}$$

III. Frequency analysis of the PWM signal

The discrete-time Fourier transform (DTFT) $Y(e^{j\omega})$ of y_n reveals the baseband content of the PWM signal and can be computed using the Hammerstein model of the digital PWM modulator in (3). Following the block diagram in Fig. 1 we have that

$$Y(e^{j\omega}) = Y_1(e^{j\omega}) + Y_3(e^{j\omega}) + Y_5(e^{j\omega}) + \cdots \tag{7}$$

where $Y_p(e^{j\omega})$ is the DTFT of the output $y_{p,n}$ of each branch of the model. The DTFTs $Y_p(e^{j\omega})$ are computed as

$$Y_p(e^{j\omega}) = W^{*p}(e^{j\omega}) H_p(e^{j\omega}) \tag{8}$$

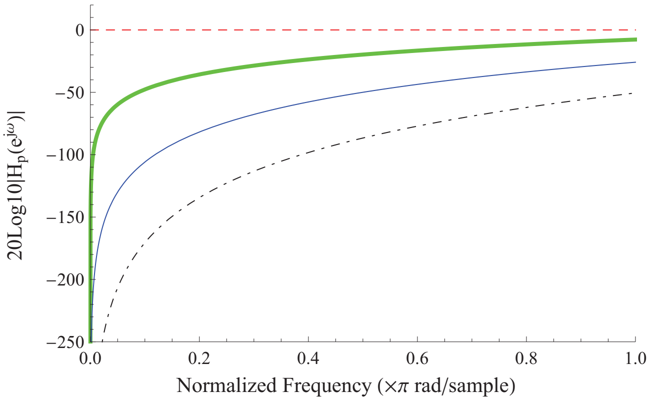

Fig. 2. Magnitude of the frequency responses $H_p(e^{j\omega})$ in dB for: $p = 1$ red, dashed; $p = 3$ green, thick; $p = 5$ blue; $p = 7$ black, dot-dashed.

where $H_p(e^{j\omega})$ is the DTFT of the impulse responses given by (6), and $W^{*p}(e^{j\omega})$ is the DTFT of $(w_n)^p$ which corresponds to the p-times periodic convolution (Modulation or Windowing Theorem) [12] of $W(e^{j\omega})$, the DTFT of w_n.

Clearly $W^{*1}(e^{j\omega}) = W(e^{j\omega})$ and the DTFT $W^{*p}(e^{j\omega})$ can be computed recursively as

$$W^{*p}(e^{j\omega}) = \frac{1}{2\pi} \int_{-\pi}^{\pi} W^{*(p-1)}(e^{j\theta}) W^{*}(e^{j(\omega-\theta)}) d\theta \tag{9}$$

for $p = 2, 3, 4, 5, \ldots$. Therefore $Y(e^{j\omega})$ is given by

$$\begin{aligned} Y(e^{j\omega}) =& W^{*1}(e^{j\omega}) H_1(e^{j\omega}) + W^{*3}(e^{j\omega}) H_3(e^{j\omega}) \\ &+ W^{*5}(e^{j\omega}) H_5(e^{j\omega}) + \cdots \end{aligned} \tag{10}$$

A. Frequency response of the filters $H_p(e^{j\omega})$

The frequency responses of the filters can be computed using its impulse responses as

$$H_p(e^{j\omega}) = \sum_{n=-\infty}^{+\infty} h_{p,n} e^{-j\omega n}, \tag{11}$$

whose closed-form expressions can be written as (see Appendix)

$$H_p(e^{j\omega}) = (j)^{p-1} \frac{\omega^{p-1}}{p!(2)^{p-1}}, \quad -\pi < \omega < \pi, \tag{12}$$

giving $H_1(e^{j\omega}) = 1$, $H_3(e^{j\omega}) = -\frac{\omega^2}{24}$, $H_5(e^{j\omega}) = \frac{\omega^4}{1920}$ and $H_7(e^{j\omega}) = -\frac{\omega^6}{322560}$ for $p = 1, 3, 5$ and 7.

Due to the symmetry of the impulse responses the frequency responses are real functions of ω. The filter $H_1(e^{j\omega}) = 1$ passes unaltered the input to the output. The higher order filters are high-pass filters with zero DC gain as shown by the magnitude responses in dB in Fig. 2.

B. Sinusoidal input

The model derived in the previous section is valid for arbitrary signals, but meaningful results can be obtained when the input x_n is a sinusoid. Given

$$x_n = A\cos(2\pi f_1 nT) = A\cos(\omega_1 n), \tag{13}$$

with $|A| < 1$ and $f_1 < f_s/2$ or equivalently $\omega_1 < \pi$, its DTFT can be written as

$$X(e^{j\omega}) = \pi A \sum_r \left[\delta(\omega - \omega_1 + 2\pi r) + \delta(\omega + \omega_1 + 2\pi r)\right], \tag{14}$$

where $\delta(\omega)$ is the Dirac impulse function. The duty cycles are

$$w_n = \frac{(1+x_n)}{2} = \frac{1}{2} + \frac{A}{2}\cos(\omega_1 n) \tag{15}$$

and its DTFT

$$W(e^{j\omega}) = \pi \sum_r \left[\frac{A}{2}\delta(\omega - \omega_1 + 2\pi r) + \frac{A}{2}\delta(\omega + \omega_1 + 2\pi r) + \delta(\omega + 2\pi r)\right]. \tag{16}$$

Using the binomial formula the powers of the duty cycles can be computed as

$$(w_n)^p = \left(\frac{1}{2} + \frac{A}{2}\cos(\omega_1 n)\right)^p = \frac{1}{2^p}\sum_{u=0}^{p}\binom{p}{u} A^u \cos^u(\omega_1 n) \tag{17}$$

where $\cos^u(\omega_1 n)$ can be expressed as the sum of its harmonics components using the trigonometric power formulas

$$\cos^{2u}(\omega_1 n) = \frac{1}{2^{2u}}\binom{2u}{u} + \frac{1}{2^{2u-1}}\sum_{k=0}^{u-1}\binom{2u}{k}\cos(2(u-k)\omega_1 n),$$
$$\cos^{2u+1}(\omega_1 n) = \frac{1}{4^u}\sum_{k=0}^{u}\binom{2u+1}{k}\cos((2u+1-2k)\omega_1 n). \tag{18}$$

Therefore, the p-th power of w_n can be expressed as

$$(w_n)^p = A_{p,0} + \sum_{k=1}^{p} A_{p,k}\cos(k\omega_1 n). \tag{19}$$

The constants $A_{p,k}$ are the amplitude of the k-th harmonic component of $(w_n)^p$.

The DTFT of $(w_n)^p$ is

$$W^{*p}(e^{j\omega}) = 2A_{p,0}\pi \sum_r \delta(\omega + 2\pi r) + \pi \sum_{k=1}^{p} A_{p,k} \sum_r [\delta(\omega - \omega_k + 2\pi r) + \delta(\omega + \omega_k + 2\pi r)] \tag{20}$$

where $\omega_k = k\omega_1$.

C. Frequency components that fall into baseband

Taking into account (10), the frequency components generated by the nonlinear behavior of the PWM modulator can be analyzed from $W^{*p}(e^{j\omega})$ in (20). We are interested in the frequency components of $W^{*p}(e^{j\omega})$ that fall in the range $0 \leq \omega < \pi$ which represents the components of the PWM signal lying in the range $0 \leq f < f_s/2$.

The input frequency ω_1 verifies that $\omega_1 < \pi$; higher frequencies generated by the PWM $\omega_k = k\omega_1$ (multiples of ω_1) will fall or not into baseband depending on the value of ω_1. Due to the 2π-periodicity of the DTFT all frequency components ω_k that do not fall into baseband will have a $2\pi r$ shifted replica noted ω_k^{bb} that falls into baseband given by

$$\omega_k^{bb} = \pi \left| \left(\left(\frac{\omega_k}{\pi} + 1\right)\right)_2 - 1 \right|, \tag{21}$$

where $((x))_n$ is the modulo operator. Figure 3 shows the mapping described by (21). This mapping of the higher frequency components into the baseband has been named as the "aliasing distortion" of the PWM modulator [3], [9]–[11].

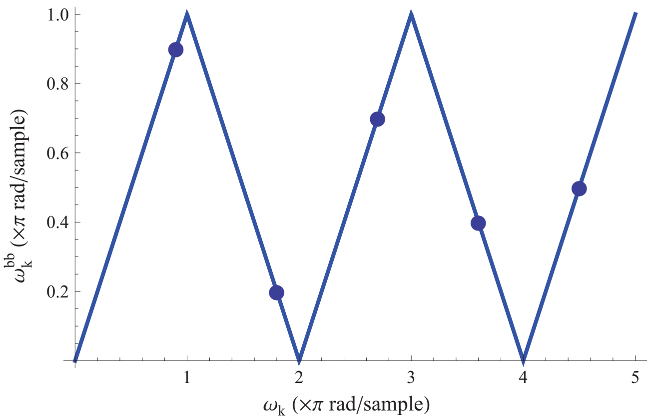

Fig. 3. Mapping of the frequencies $\omega_k = k\omega_1$ into the frequencies ω_k^{bb}. The dots indicate the mapping for $\omega_1 = 0.9\pi$.

TABLE I
EXAMPLE OF THE BASEBAND FREQUENCIES GENERATED BY $W^{*p}(e^{j\omega})$ FOR $\omega_1 = 0.04\pi$, $\omega_1 = 0.2\pi$ AND $\omega_1 = 0.9\pi$.

	In freq.	Baseband frequencies			
$W^{*p}(e^{j\omega})$	ω_1	ω_2^{bb}	ω_3^{bb}	ω_4^{bb}	ω_5^{bb}
$W^{*1}(e^{j\omega})$	0.04π	–	–	–	–
	0.2π	–	–	–	–
	0.9π	–	–	–	–
$W^{*3}(e^{j\omega})$	0.04π	0.08π	0.12π	–	–
	0.2π	0.4π	0.6π	–	–
	0.9π	0.2π	0.7π	–	–
$W^{*5}(e^{j\omega})$	0.04π	0.08π	0.12π	0.16π	0.24π
	0.2π	0.4π	0.6π	0.8π	π
	0.9π	0.2π	0.7π	0.4π	0.5π

Example of frequency mapping into baseband: For a fifth-order model, an input of frequency ω_1 produces the frequency components ω_2, ω_3, ω_4 and ω_5 that map into the frequencies ω_2^{bb}, ω_3^{bb}, ω_4^{bb} and ω_5^{bb}. Table I shows the mapping for three values of input frequency: low ($\omega_1 = 0.04\pi$), medium ($\omega_1 = 0.2\pi$) and high ($\omega_1 = 0.9\pi$).

For $\omega_1 = 0.04\pi$ and $\omega_1 = 0.2\pi$ Table I shows that $\omega_k^{bb} = \omega_k = k\omega_1$. For the high frequency signal $\omega_1 = 0.9\pi$ the frequency components are located according to (21) as indicated by the dots in Fig. 3, these components are known as "aliasing distortion" of the PWM modulator.

D. Amplitudes of the components generated by each branch and by the complete PWM output

The amplitudes $A_{p,k}$ of the ω_k frequency components of $(w_n)^p$ decreases for growing values of k. Table II shows the amplitude $A_{p,k}$ of the frequency components generated by each of the $W^{*i}(e^{j\omega})$ branches considering upto $p = 5$. For example, the linear branch only generates the fundamental component with amplitude $A_{1,1} = A/2$ while the cubic branch $W^{*3}(e^{j\omega})$ contributes to the fundamental with amplitude $A_{3,1} = (12A + 3A^3)/32$ but also generates

TABLE II

GENERAL FORMULAS FOR THE AMPLITUDE OF THE FREQUENCY COMPONENTS GENERATED BY $W^{*p}(e^{j\omega})$.

$W^{*p}(e^{j\omega})$	$A_{p,1}$	$A_{p,2}$	$A_{p,3}$	$A_{p,4}$	$A_{p,5}$
$W^{*1}(e^{j\omega})$	$\frac{A}{2}$	–	–	–	–
$W^{*3}(e^{j\omega})$	$\frac{(12A+3A^3)}{32}$	$\frac{3A^2}{16}$	$\frac{A^3}{32}$	–	–
$W^{*5}(e^{j\omega})$	$\frac{(80A+120A^3+10A^5)}{512}$	$\frac{(80A^2+40A^4)}{512}$	$\frac{(40A^3+5A^5)}{512}$	$\frac{5A^4}{256}$	$\frac{A^5}{512}$

TABLE III

GENERAL FORMULAS FOR THE AMPLITUDE OF THE PWM COMPONENTS.

Name	Amplitude
A_1	$\frac{A\left(49152-384\left(4+A^2\right)(\omega_1)^2+\left(8+12A^2+A^4\right)(\omega_1)^4\right)}{98304}$
A_2	$\frac{A^2(\omega_2^{bb})^2\left(-192+\left(2+A^2\right)(\omega_2^{bb})^2\right)}{24576}$
A_3	$\frac{A^3(\omega_3^{bb})^2\left(-256+\left(8+A^2\right)(\omega_3^{bb})^2\right)}{196608}$
A_4	$\frac{A^4(\omega_4^{bb})^4}{98304}$
A_5	$\frac{A^5(\omega_5^{bb})^4}{983040}$

second and third harmonics with amplitudes $A_{3,2} = 3A^2/16$ and $A_{3,3} = A^3/32$ respectively. The branch filters (Fig. 1) further attenuates the amplitudes of the harmonics.

The complete output y_n representing the baseband content of the PWM signal using the model of order 5 is

$$
\begin{aligned}
y_n = &\frac{1}{2} + A_1 \cos(\omega_1 n) + A_2 \cos(\omega_2^{bb} n) + A_3 \cos(\omega_3^{bb} n) \\
&+ A_4 \cos(\omega_4^{bb} n) + A_5 \cos(\omega_5^{bb} n)
\end{aligned}
\tag{22}
$$

where A_k is the amplitude of the ω_k^{bb} component in the PWM signal. Each A_k has contributions from different branches of the model weighted by the amplitude gain of the filter $H_p(e^{j\omega})$ of each branch. Since for the PWM model the frequency responses of the filters are real functions of ω then

$$
A_k = A_{1,k} H_1(e^{j\omega_k^{bb}}) + A_{3,k} H_3(e^{j\omega_k^{bb}}) + A_{5,k} H_5(e^{j\omega_k^{bb}}). \tag{23}
$$

Table III shows the formulas for the computation of A_k for any sinusoidal input of frequency ω_1 and amplitude A.

E. Total Harmonic Distortion

Using the results in Table III the Total Harmonic Distortion (THD) generated by the pulse width modulator can be computed analytically. The THD is defined as

$$
\begin{aligned}
\text{THD} &= \frac{\sqrt{A_2^2 + A_3^2 + A_4^2 + A_5^2}}{A_1} \\
&= \frac{\sqrt{a_2 A^2 + a_4 A^4 + a_6 A^6 + a_8 A^8}}{b_0 + b_2 A^2 + b_4 A^4}
\end{aligned}
\tag{24}
$$

where A is the amplitude of the input sinusoidal; the coefficients of the numerators are:

- $a_2 = 58982400(\omega_2^{bb})^4 - 1228800(\omega_2^{bb})^6 + 6400(\omega_2^{bb})^8$
- $a_4 = -614400(\omega_2^{bb})^6 + 6400(\omega_2^{bb})^8 + 1638400(\omega_3^{bb})^4 - 102400(\omega_3^{bb})^6 + 1600(\omega_3^{bb})^8$
- $a_6 = 1600(\omega_2^{bb})^8 - 12800(\omega_3^{bb})^6 + 400(\omega_3^{bb})^8 + 100(\omega_4^{bb})^8$
- $a_8 = 25(\omega_3^{bb})^8 + (\omega_5^{bb})^8$

and the coefficients of the denominator:

- $b_0 = 491520 - 15360(\omega_1)^2 + 80(\omega_1)^4$
- $b_2 = -3840(\omega_1)^2 + 120(\omega_1)^4$
- $b_4 = 10(\omega_1)^4$.

Figure 4 shows the THD [%] as a function of the frequency $0 \le \omega < \pi$ obtained analytically with (24). The THD [%] is shown for three values of amplitude A, also know as the modulation depth or modulation index: $A = 0.5$ (red-thick), $A = 0.75$ (green-dashed) and $A = 0.95$ (blue-dot-dashed). Distortion is higher when A grows but has an irregular behavior as a function of frequency ω:

- For $0 \le \omega < \pi/2$ the THD [%] grows reaching maximums of 7.45%, 11.1% and 13.88% for the three values of A. In this region the THD [%] is dominated by the harmonic frequencies generated by the digital PWM modulator (mainly $\omega_2^{bb} = 2\omega_1$).
- At $\omega = \pi/2$ all baseband frequencies ω_k^{bb} fall either at π or at $\pi/2$ so that there is no distortion component in $0 \le \omega < \pi$: the THD [%] is zero at this point.
- For $\pi/2 < \omega < \pi$ distortion is generated by carrier side-bands that fall into baseband ("PWM aliasing-distortion").

Simplified THD: For $\omega_1 < \pi/2$ the THD can be approximated by

$$
\text{THD} \approx \frac{1}{16} A (\omega_1)^2 \tag{25}
$$

with an error of less than 1%. Equation (25) shows that in this region the THD is proportional to the input amplitude (modulation index) A and to the square of the input frequency ω_1.

Example of PWM used for a switched audio amplifier: The input frequency ranges from 20 Hz to 20 kHz; if the PWM frequency is $f_s = 80$ kHz then the maximum value for $\omega_1 = 2\pi 20000/80000 = \pi/2$ and hence (25) revels that the expected THD considering the distortion in frequency range 0 to 40 kHz is less than 11.6% for $A = 0.75$. On the other hand, if $f_s = 300$ kHz, which is a typical value for switched audio amplifiers, then the maximum value for $\omega_1 = 2\pi 20000/300000 = 2\pi/15$ and (25) gives that the THD is less than 0.82% considering the distortion components in the frequency range 0 to 150 kHz.

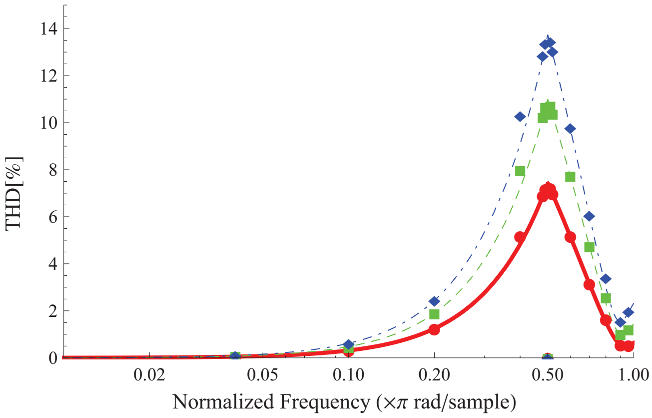

Fig. 4. Analytically computed curves for THD [%] as a function of $0 < \omega/\pi < 1$ for $A = 0.5$ (red-thick), $A = 0.75$ (green-dashed) and $A = 0.95$ (blue-dot-dashed). The dots, squares and diamonds indicates the results of a numerical simulation.

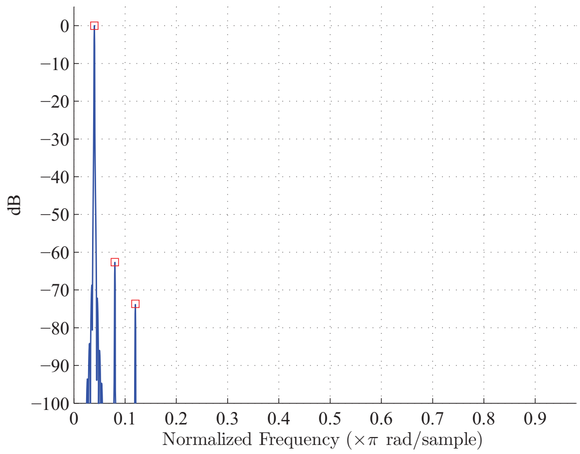

Fig. 5. Spectra obtained with the analytical model (squares) and with the numerical simulation (solid line). $\omega_1 = \pi/25$, $A = 0.75$.

IV. Simulations

To verify the results for the THD [%] obtained by equation (24) a numerical simulation of the PWM modulator was performed. The actual two-level $q(t)$ signal is generated, low pass filtered to avoid aliasing and sampled to compute the FFT. The simulation time for each frequency and amplitude is long, since the PWM signal should have enough time-resolution to achieve quantization noise below -100 dB, and also because several periods of the input signal must be simulated to obtain a spectrum with good frequency resolution. Using the FFT, a frequency band around the fundamental frequency is selected as the input and all the remaining spectra in the range $0 \leq \omega < \pi$ is considered as distortion. This procedure is equivalent to the computation of total harmonic distortion plus noise (THD+N) typically performed by spectral analyzers. Since it is expected that noise is several orders of magnitude lower than the harmonic components, the THD+N is similar to THD in our case.

A very good match between the analytical results (curves) and the simulations results (dots) of the THD are shown in Fig. 4 for three amplitude values.

Figures 5 to 8 show the spectra obtained with the numerical simulations (curves) and computed with the analytical expressions (dots) in Table III for $A = 0.75$.

- For $\omega_1 = \pi/25$ and $\omega_1 = 0.2\pi$ the spectra in Fig. 5 and Fig. 6 shows that spurious components appear at multiples of the input frequencies (harmonics).
- For $\omega_1 = \pi/2$ no distortion components appear in baseband ($\omega < \pi$). This can be observed in Fig. 7 and corresponds to the zero THD point in Fig. 4.
- For frequencies greater than $\pi/2$ distortion components appear as aliasing distortion. For $\omega_1 = 0.9\pi$ the spectra is shown in Fig. 8.

In all cases the analytic results using upto the power $p = 5$ (summarized in Table III) perfectly match the numerical simulations of the real PWM modulator.

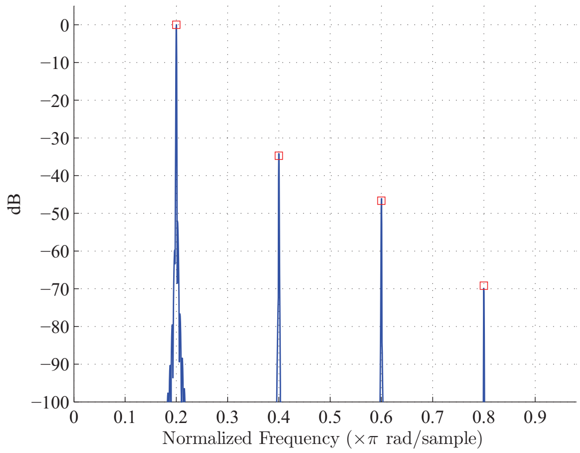

Fig. 6. Spectra obtained with the analytical model (squares) and with the numerical simulation (solid line). $\omega_1 = \pi/5$, $A = 0.75$.

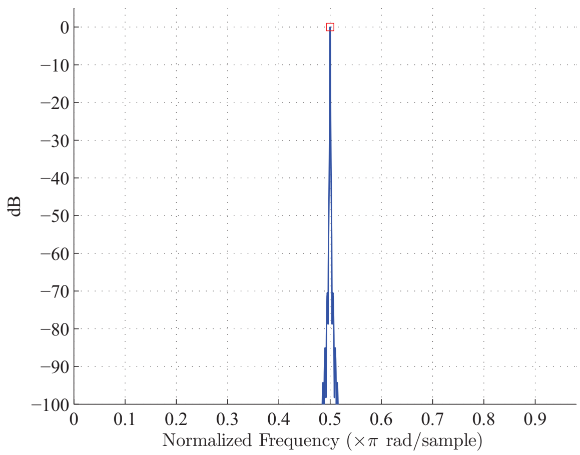

Fig. 7. Spectra obtained with the analytical model (squares) and with the numerical simulation (solid line). $\omega_1 = \pi/2$, $A = 0.75$.

V. Conclusions

A model for digital PWM composed of odd powers and digital filters was reviewed. Closed-form formulas for the impulse and frequency responses of the filters of any order

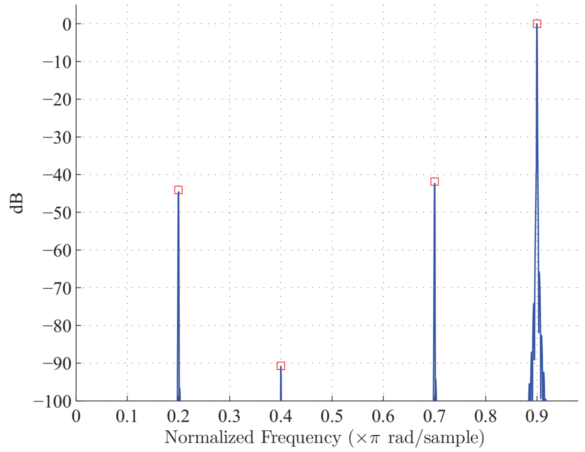

Fig. 8. Spectra obtained with the analytical model (squares) and with the numerical simulation (solid line). $\omega_1 = 0.9\pi$, $A = 0.75$.

p were presented. The model allowed to perform a frequency analysis of the PWM modulator that was useful to identify the frequencies and amplitudes that appear in the baseband. These components were used to compute the THD which, under typical practical conditions, is proportional to the modulation index and to the square of the input frequency. Simulations showed that a 5-th order model is enough to capture the baseband behavior of the modulator. The proposed model can also be used to speed up simulations of a PWM modulator.

Appendix
Frequency responses of the filters

We show that the expression for $H_p(e^{j\omega})$ in (12) correspond to the impulsive response $h_{p,n}$. The definition of the inverse DTFT transform states that

$$\begin{aligned} h_{p,n} &= \frac{1}{2\pi}\int_{-\pi}^{\pi} H_p(e^{j\omega})e^{j\omega n}d\omega \\ &= \frac{(j)^{p-1}}{2\pi p!(2)^{p-1}}\int_{-\pi}^{\pi}\omega^{p-1}e^{j\omega n}d\omega. \end{aligned} \tag{26}$$

To solve the integral in (26) the cases $n \neq 0$ and $n = 0$ are analyzed separately. For $n = 0$ the result is

$$h_{p,0} = \frac{1}{pp!}\left(\frac{\pi}{2}\right)^{p-1}\sin\left(\frac{p\pi}{2}\right). \tag{27}$$

The primitive function of the integral for $n \neq 0$ is

$$F(\omega) = \int \omega^{p-1}e^{j\omega n}d\omega = e^{jn\omega}\sum_{u=0}^{p-1}\frac{(p-1)!(-1)^{p-1-u}}{u!(jn)^{p-u}}\omega^u. \tag{28}$$

The impulse responses for $n \neq 0$ can be found by using the primitive

$$\begin{aligned} h_{p,n} &= \frac{(j)^{p-1}}{2\pi p!(2)^{p-1}}\left(F(\pi) - F(-\pi)\right) \\ &= \frac{j(-1)^{n+p}}{p\pi 2^p n^p}\sum_{u=0}^{p-1}\frac{(j\pi n)^u}{u!}\left((-1)^u - 1\right). \end{aligned} \tag{29}$$

This gives the general expression for the computation of the impulse responses shown in (6).

References

[1] D. Holmes and T. Lipo, *Pulse width modulation for power converters: principles and practice*. John Wiley & Sons, 2003, vol. 18.

[2] C. Pascual, Z. Song, P. Krein, D. Sarwate, P. Midya, and W. Roeckner, "High-fidelity PWM inverter for digital audio amplification: Spectral analysis, real-time DSP implementation, and results," *IEEE Trans. Power Electron.*, vol. 18, no. 1, pp. 473–485, Enero 2003.

[3] K. Hausmair, S. Chi, P. Singerl, and C. Vogel, "Aliasing-free digital pulse-width modulation for burst-mode RF transmitters," *IEEE Trans. Circuits Syst. I, Reg. Papers*, vol. 60, no. 2, pp. 415–427, Feb 2013.

[4] F. Chierchie and E. Paolini, "Real-time digital PWM with zero baseband distortion and low switching frequency," *IEEE Trans. Circuits Syst. I, Reg. Papers*, vol. 60, no. 10, pp. 2752–2762, Octubre 2013.

[5] F. Chierchie, E. Paolini, L. Stefanazzi, and A. Oliva, "Simple real-time digital PWM implementation for class-D amplifiers with distortion-free baseband," *IEEE Trans. Ind. Electron*, vol. 61, no. 10, pp. 5472–5479, Octubre 2014.

[6] S. Aase, "Digital removal of pulse-width-modulation-induced distortion in class-D audio amplifiers," *IET Signal Processing*, vol. 8, no. 6, pp. 680–692, Agosto 2014.

[7] F. Chierchie and S. Aase, "Volterra models for digital PWM and their inverses," *IEEE Trans. Circuits Syst. I, Reg. Papers*, vol. 62, no. 10, pp. 2606–2616, Octubre 2015.

[8] Z. Song and D. Sarwate, "The frequency spectrum of pulse width modulated signals," *Signal Processing*, vol. 83, no. 10, pp. 2227–2258, Octubre 2003.

[9] S. Santi, R. Rovatti, and G. Setti, "Spectral aliasing effects of PWM signals with time-quantized switching instants," in *Proceedings of the International Symposium on Circuits and Systems, ISCAS.*, vol. 4, May 2004, pp. IV–689–92 Vol.4.

[10] A. M. A. Amin, M. I. El-Korfolly, and S. A. Mohammed, "Exploring aliasing distortion effects on regularly-sampled PWM signals," in *3rd IEEE Conference on Industrial Electronics and Applications, ICIEA.*, June 2008, pp. 2036–2041.

[11] K. Hausmair, P. Singerl, and C. Vogel, "Multiplierless implementation of an aliasing-free digital pulsewidth modulator," *IEEE Trans. Circuits Syst. II, Exp. Briefs*, vol. 60, no. 9, pp. 592–596, Sept 2013.

[12] A. Oppenheim and R. Schafer, *Discrete-Time Signal Processing*. Prentice Hall, New Jersey, 1989.